Towards half-moon-shaped soft pneumatic cilia

Edoardo Milana, Sam Peerlinck, Sean Flaherty, Dominiek Reynaerts and Benjamin Gorissen

Abstract— **Symmetry breaking mechanisms lead to locomotion with a reduced number of inputs, with soft robotic solutions emerging for both terrestrial and aquatic propulsion [1], [2]. For fluids, natural cilia are a source of inspiration that display an asymmetric actuation cycle where the forward and backwards stroke are following a different path. To instigate a similar path asymmetry, this paper reports on the design, simulation, fabrication and characterization of a soft bending pneumatic actuator with an unconventional half-moon shaped cross-section. The cross-section is constant along the actuator length and a design is proposed where both the outer profile and the inflatable inner cavity are half-moon shaped. The actuator is dimensionalised trough iterative structural simulations performed with Ansys simulation software, optimising the bending angle and the compatibility with a low Reynolds environment when submerged in a fluid with high viscosity. The actuator is fabricated through a single-step molding process out of silicone rubber. In order to obtain the complex geometry, the mold is made out of multiple aluminium components that are machined with wire electrical discharge machining and conventional milling. An experimental characterization is performed, analysing both the pressure-volume and the bending-angle characteristic. Results show that the actuator achieves a bending angle of about 60° at 50 kPa with a constant curvature. Structural simulations reveal that the corners of the half-moon cross-sections are stress-free, which is optimal in the perspective of coupling in hydrodynamic forces to change the cross section while being submerged in a liquid.**

I. Introduction

Cilia are slender organelles that protrude out of the cell body and occur in biological systems such as mammal lung trachea, oviducts, hearing channels, etc. [3]. Cilia are responsible for the locomotion of microorganism or for the generation and detection of fluid flows. When flow generation is the objective, these hair-like active structures display a typical asymmetric movement. Besides a global actuation asymmetry where neighboring cilia beat at a phase difference to create metachronal waves, a single cilium exhibits path asymmetry where the tip of the cilium sweeps an area during a full actuation period [4]. These asymmetries are necessary to propel fluid at low Reynolds number conditions, which they observe due to their small scale. At low Reynolds numbers, the inertial forces in the fluid are dominated by the viscous forces, requiring the observed asymmetric movements of cilia to impose a fluid flow [5]. Researchers have been trying to replicate these asymmetric movements with artificial cilia over the past decades, foreseeing possible applications for microfluidic pumps or microrobotic swimmers [6].

In recent years there has been an cross-over between soft robotics and artificial cilia research, as soft actuators are regularly used to impose bending deformations that are similar to the deformation of natural cilia. Many new designs of pneumatic [7], [8] and magnetic [9], [10] artificial cilia have been shown reported in literature that use materials and fabrication processes that are typically adopted for large-scale soft robotics, such as soft silicone rubbers (e.g. Ecoflex, PDMS) and molding processes [11]. While the first generation of artificial cilia was based on lithographic fabrication processes and focused on targeting micrometer sizes, this new generation of cilia gives priority to generating asymmetric movements, thanks to the compliance of the miniaturised soft actuators [12].

Harnessing the principles of pneumatic actuation, in previous works we developed two-degree-of-freedom artificial cilia that incorporated two sections with each a different soft bending pneumatic actuator [7], [12]. These two actuators are individually addressed with a phase difference to create the necessary asymmetric movement of the cilium, inducing low Reynolds fluid flow in a way that the swept area can be carefully controlled. However, individual addressable segments require dedicated peripherals (pressure regulators, valving, tubing) for each segment. Further, the addition of a second segment in the same structure drastically increases manufacturing complexity, reducing the potential for scale reduction. Solutions where the same motion asymmetry can be generated while only needing one pressure supply tube are thus of high importance, opening up avenues for scaling up production to create ciliary carpets with a significant number of cilia to approach the architecture of natural cilia systems.

In this paper, we investigate a new design of an artificial cilium with a half-moon shaped cross section. We hypothesize that differential hydrodynamic forces during forward stroke and backwards stroke instigate the needed motion asymmetry for fluid propulsion. First, we will elaborate the design of such half-moon shaped cilium, describing on its symmetry breaking mechanism. Further, we dimensionalise the cilium through iterative finite element simulations to assess the structural bending movement. Lastly we corroborate these results by tests on a prototype actuator and give recommendations for future work.

II. Design

It is necessary that a single cilium displays spatial asymmetry between the effective (in the direction of the net fluid flow) and recovery stroke (against the direction of the net fluid flow) in order to generate a net fluid flow in a tangential direction. So far, this asymmetry has mainly be obtained by introducing tip trajectory asymmetry, which means that the tip of cilium sweeps an area in the plane of beating, by following a different trajectory between the two strokes. In order to reduce the number of fluidic inputs for a single cilia to one, we deviate from the traditional eccentric circle cross

All authors are with Department of Mechanical Engineering, KU Leuven, Leuven, Belgium and members of Flanders Make.

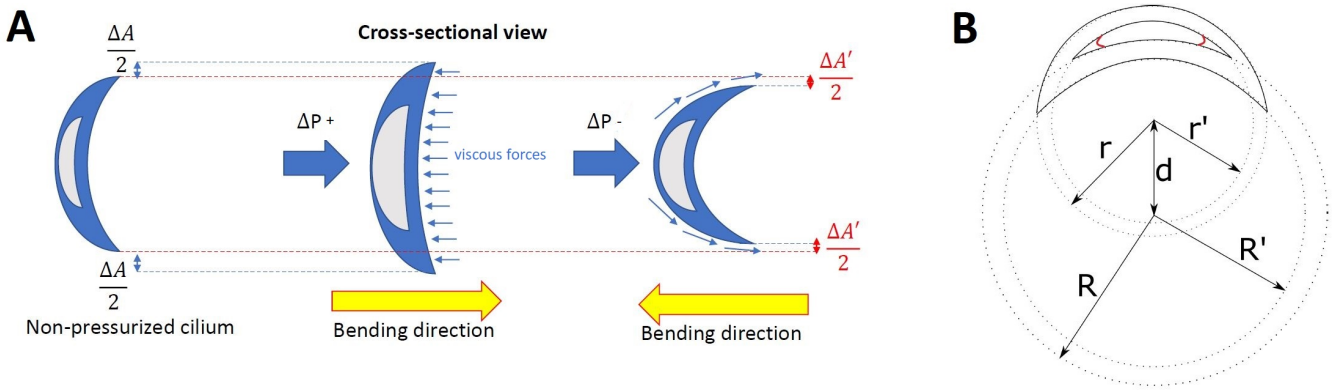

Fig. 1. A. Illustration of the theorized surface asymmetry that occurs during effective and recovery stroke. B. Definition of the halfmoon shape based on five parameters. The roundings in the cavity are marked in red.

section [13] to a half-moon shaped cross section. Although this geometry would not cause any asymmetry just by being actuated, we hypothesize that forces from the interaction with the fluid will alter the cross sectional geometry that is different depending on the direction of the relative fluid flow. To our knowledge, this type of asymmetry is not present in natural cilia that are all symmetric in cross section, and will further be labeled as surface asymmetry. This surface asymmetry originates from the asymmetric shape of the half-moon shaped cilium seen by the fluid. This makes the cilium undergo a different interaction with the fluid during effective and recovery stroke.

The idea behind this is illustrated in Figure 1A. During the effective stroke the cilium acts as a flexible spoon which opens up the surface of the cilium by interaction with the fluid. Since the cilium is designed to operate at low Reynolds flow conditions, the drag by viscous forces has the potential to deform the soft structure of the cilium, if designed properly. This enlarged projected surface will be able to impose forces to a larger fluidic domain compared to in its undeformed shape. On the contrary, the recovery stroke will experience a reduction of the surface subjected to the drag. This is caused again by interaction with the viscous forces and in this case the flexible cilium is squeezed together. During this stroke, the fluid experiences forces from a smaller object. Since the projected surface along the net flow direction is larger during the effective stroke compared to the recovery stroke, the amount of fluid moved is different and therefore a net fluid flow can be expected. This hypotheses can be assessed at different length scales as long as we keep the Reynolds number constant and in the range of previously validated solutions (0.1-10) [12]. For ease of manufacturing we start to explore surface asymmetry at a centimeter length scale.

III. Parametrization and Finite Element Simulations

We choose a fixed cross-section along the length of the cilium, reducing parameterisation to the 2D domain. The parametric representation of the cross section uses five parameters that define an inner cavity and outer boundary of the cilium, as shown on Figure 1B. The bending motion originates from a eccentricity between the inflatable inner cavity and the rest of the structure [14]. The first parameter d gives the distance between two center points of pairs of circles. Each center point has two concentric circles with the radii of the first pair defined as r, r' and the second pair R,R'. Figure 1B shows how the cross-section (solid black lines) that can be found based on the intersections of these circles. The two sharp points created in the inner cavity would be very sensitive to tearing under numerous beating cycles of the cilium and are therefore rounded to reduce stress concentrations. This rounding is characterized by a radius and can be seen as an additional parameter, depicted in red on figure 1B.

The actual values of the parameters are estimated using finite element simulations. Design iterations have been conducted to determine geometrical parameters that satisfy the constraints on the Reynolds number, needed to lay between $(0.1 - 10)$, which will be explained later on. Simulations are performed in Ansys, through the static structural functionality. The cilium in this work is made of Dragon Skin 30 which is a bi-component silicone rubber. A hyperelastic Ogden model is used to simulate the Dragon Skin 30 with the following parameters $\alpha_1 = 5.836$, $\mu 1 = 0.075449$ MPa [15]. To ease the computational load, the tip trajectory is analytically approximated considering the resting point of the tip and its position at the maximum load, by assuming a constant curvature bending and an invariable length. At the end of the iterative process, we identified a set of lengths (L = 27-77 mm) and tip trajectories (Δs) that are compatible with the requirement on the Reynolds number, while being actuated at maximum pressure of 40 kPa. We also verified that the maximum strains during loading are below the ultimate tensile strain of Dragon Skin 30, incorporating a safety factor of 30%.

For these found configurations, the cross-sectional parameters are listed in table 1. Figure 2A depicts the tip trajectories for the set of lengths and figure 2B depicts the variation of the Reynolds number for the different lengths and for different time strokes (T = 0.5, 1, 2 s). The Reynolds number is computed using the following equation:

$$Re = \frac{\Delta s L}{T \nu}, \tag{1}$$

where ν is taken to be the kinematic viscosity of glycerol ($1.138 \cdot 10^{-3}$ m^2/s at 20 °C).

IV. Fabrication

The cilium is made out of Dragon Skin 30 through a one-step molding process, avoiding bonding interfaces that act as structural weak spots. Given the unusual asymmetric shape of the cross-section and of the inner cavity of our cilia-actuator, the fabrication process requires a complex design of the mold.

A. Mold manufacturing

The mold is composed of two main components, a large half-moon shaped cavity to shape the outer dimensions of the cilium and a rod with a half-moon cross-section that corresponds to the inflatable inner cavity. Both components are made out of aluminium. Figure 3 shows a photo of the

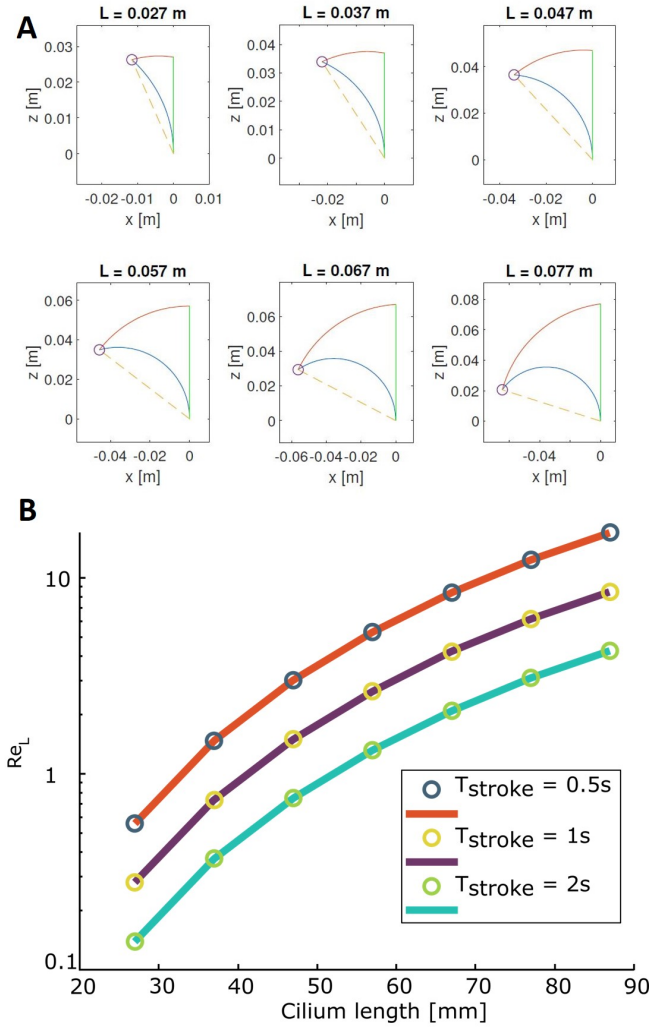

Fig. 2. A. The approximated tip trajectory is given by the red curve. The vertical green line represents the cilium at rest and the blue curved line the approximated final bent state of the cilium at maximum operating pressure. B. The Reynolds number Re in function of the cilium length and stroke time.

TABLE I
Cross-sections dimensions of the parameters depicted in figure 1B

Parameter	Value (mm)
r	8
r'	7.5
R	11
R'	10
d	5

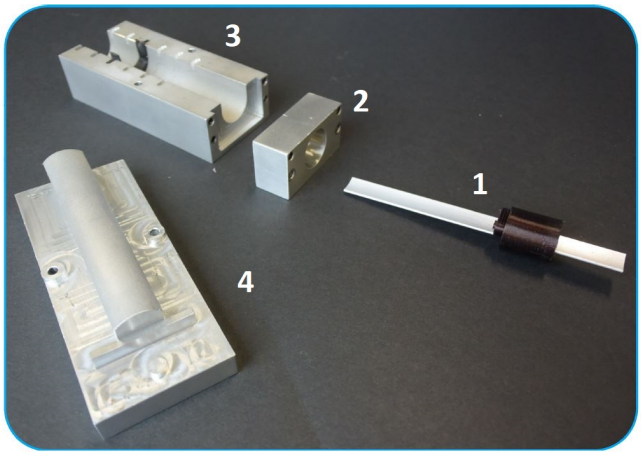

Fig. 3. Disassembled mold, consisting of half-moon rod with holder (1), rod holder fit (2) and half-moon negative profile (3) of the bottom mold, and the top mold (4).

multiple parts of the mold. The mold is constructed in such a way to accommodate different lengths of the actuator: the rod holder can slide over the internal rod to set the depth of the internal void; and a length-setting piece can adjust the outer length. Both rod holder and length-setting piece are fabricated via 3D printing. The internal rod (referred as 1 in the figure) is cut out of an aluminium piece using wire electrical discharge machining (EDM). The rod slides in the mold cavity at different depths using the rod holder, enabling the manufacturing of the cilia with the different lengths as discussed in the Design section. The mold cavity is assembled out of four parts, two for the top mold and two for the bottom mold. The bottom mold features a half-moon shaped negative profile realized through EDM (3), with a milled feature to fit the rod holder (2). The top mold is made of a rectangular support made by milling and half-moon shaped profile made by wire EDM (4). Additional features are machined through milling, such as the alignment- and screw holes and the slots for the length-setting piece.

B. Cilium casting

The first step of the casting process is the insertion of the rod that shapes the actuator's cavity in the bottom mold. The depth of that cavity and the desired length of the cilium are controlled through the length-setting piece and the rod holder. The pre-cured Dragon Skin 30 blend is prepared by

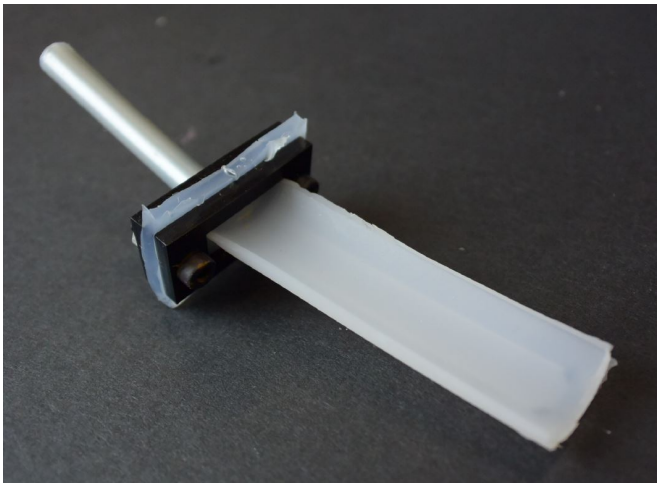

Fig. 4. Image of the fabricated cilium with the pressure-line connection.

mixing the two components in a 1:1 ratio in a cup. The cup is then placed in a vacuum chamber for 5 minutes to extract the air bubbles trapped in the viscous blend. The degassed blend is slowly poured in the half-moon shaped cavity of the bottom mold. The bottom mold with the liquid rubber is subsequently placed for a second degassing round in the vacuum chamber for 10-15 minutes. This step is critical because tiny air bubbles may be trapped between the rod and the surface of the mold, resulting in structural defects or even holes in the final device. The top mold is then placed on the full bottom mold by means of alignment pins and tightened to the bottom mold using screws. When tightening the two parts together, the excess rubber is pushed outside the mold, making sure that the cavity forming the cilium is completely filled. The mold is placed in the oven at 55 °C for 45 minutes to let the rubber cure. The demolding step is supported by the use of ethanol as lubricant, in particular to extract the rod from the formed cilium. The fabricated cilium with the pressure-line connection is displayed in it's unactuated state on figure 4.

V. Characterization

In this section we detail the results of the structural simulation and of the experimental characterization for a half-moon shaped cilium with a length of 57 mm.

A. Simulation

The resulting deformed configuration and Von-Mises stress-field, determined with the structural simulation for a input pressure of 40 kPa, is depicted in figure 5. High tensile strains are reported along the outside edge which was designed to be the thinnest. The flaps of the cilium are sufficiently far removed from the pressurized cavity to not be influenced by its deformation and remain stress-free. This means that if the cilium is to be surrounded with a viscous fluid, the cilium flaps are highly susceptible to hydrodynamic forces that do not have to counter any pre-tension. This will likely improve the possibility of a significant surface change as explained in first paragraph of the Design section. The quasi-static volume curve (PV curve) of the actuator is obtained by post-processing the deformation results of multiple simulations at different pressure points. The simulated curve

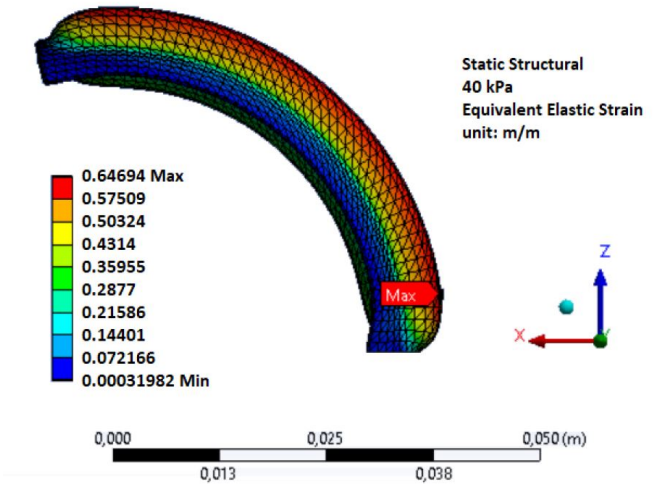

Fig. 5. Illustration of the FEM simulated strain field for an operating pressure of 40 kPa.

(figure 6A) is monotonically increasing. From this graph the following conclusions can be drawn: the pressure does not change much for lower volumes but starts increasing faster from 0.5 to 1.5 cm^3. For volumes higher than 1.5 cm^3 the PV curve has a nearly constant slope with a slightly decreasing tendency. The curve was set up for pressures up to 57 kPa, where the theoretical elongation at break is reached, based on the Von-Mises yield criterion.

Figure 6B shows the tip's coordinates trajectory, obtained with the same multiple simulations as for the PV curve. The simulated tip trajectory shows some peculiarities, compared to the constant curvature approximation in the design phase. The tip first remains approximately at a constant vertical level while moving backwards horizontally, against the desired fluid direction. This indicates that the cilium is slightly elongating when it initially inflates. Indeed, for the rest of the trajectory, the simulated tip moves higher than the approximated arc of circumference, as we discuss further.

B. Experimental

In order to experimentally characterize the bending deformation and the tip trajectory, the cilium is connected to an electro-pneumatic valve to accurately control the actuation pressure. The pressure was ramped up to 50 kPa which is higher than the 40 kPa fixed in the simulation. This higher pressure is only used for the validation of the simulated and approximated bending angle and not for cyclic loading. The ultimate bending deformation is shown in figure 7. An image analysis process is used to determine the ultimate bending angle. The experimental bending angle is approximately 58.5°. The comparison of this bending angle can be done with the simulated curve for the bending angle in function of supplied pressure 6C. The value read from this graph is 62.49°. The bending angle is therefore slightly different probably due to dimensional errors during the production of the cilium. A small deviation in the wall thicknesses of the recovery or effective edge can lead to quite a difference in bending angle.

A video analysis was also made of the bending of the cilium under this pressure ramp. The video can be decom-

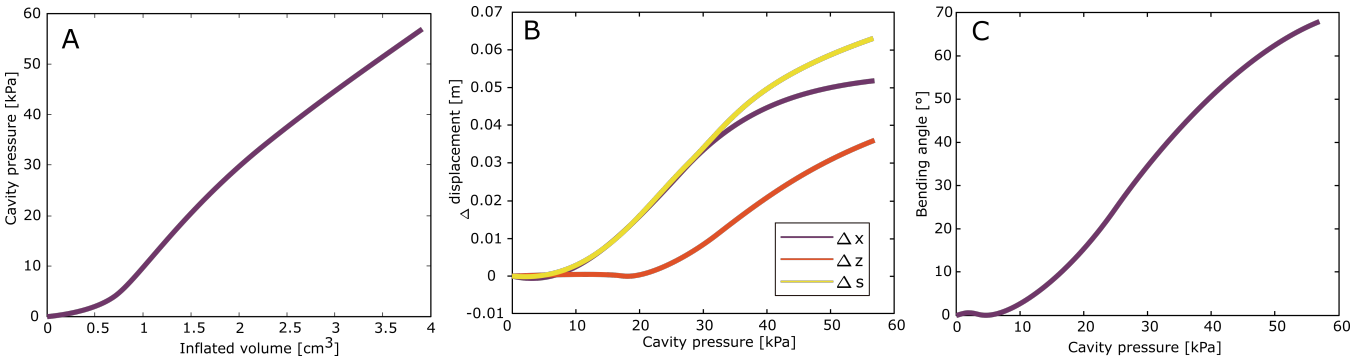

Fig. 6. A. Simulated pressure-volume curve for a cilium with length 57 mm. B. Simulated tip coordinates and displacement at corresponding different supply pressures for a cilium with length 57 mm. C. Simulated bending angle in function of pressure for a cilium with length 57 mm.

Fig. 7. Bending deformation for a cilium with length 57 mm at a pressure of 50 kPa.

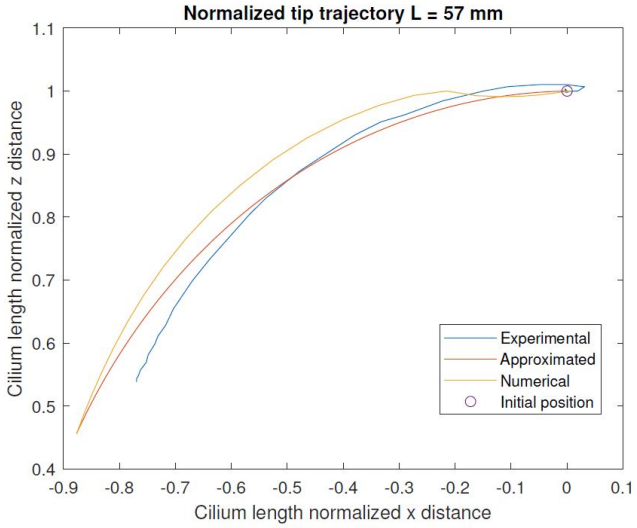

Fig. 8. Graph showing the simulated, approximated and experimental tip trajectories. The simulated and approximated trajectories are normalized for a maximum pressure of 50 kPa. The ultimate tip position of the experimental curve is also for a pressure of 50 kPa.

posed in frames which can then be converted to binary valued frames. This is very useful because of the bright appearance of the cilium against its background. A filter is used to get rid of white surfaces that are too small too be part of the cilium. The tip trajectory can then easily be followed because of the contrast between cilium and background. The tip position is then normalized with the cilium length (57 mm). This normalized tip trajectory is graphically shown in figure 8. The approximated tip trajectory and the simulated tip trajectory are also normalized for this length and presented in the same graph. As mentioned in the previous paragraph, this comparison depicts the higher position of the simulated tip compared to the approximation. Interestingly, the negative bending angle that was observed during the simulation is also observed in the experiment.

In a second test to obtain the real pressure-volume curve, the cilium is connected to a motorized syringe pump. The actuation fluid used is water because it is nearly incompressible, making it easy to control the volumetric increase of the actuator cavity. The pressure-volume curve is given in figure 9 for a cilium with length 57 mm. The curve is measured over a whole beating cycle, so effective and recovery stroke. The first thing to notice is that no leaks are present anywhere in the system. The reason for this is that the final point coincides with the starting point. One of the larger differences with the simulated PV-curve is the occurrence of a hysteresis loop. This can interpreted as elastic energy lost by friction between the silicone microstructures. Indeed, the material model used in the simulations does not take this effect into consideration and thus no hysteresis can be observed in the simulation results. The maximum volume that was injected is 5 ml and corresponds to a unique pressure of 42.24 kPa. Comparing this with the simulated graph in figure 6A, the volume injected at the same pressure is 2.83 ml. The simulated volume for that pressure is less than the experimental. This can be probably caused by an overestimation of the stiffness of Dragon Skin 30 in the material model used in the simulations. In fact, the inner cavity in the experiment undergoes larger volumetric increases due to the higher stretches of the half-moon shape membranes. The effect of the material model is more noticeable because the model was not meshed as fine over the wall thickness compared to the length of the cilium. The high aspect ratio between these wall thicknesses and the length causes the meshing to be challenging. A fine mesh in these walls would strongly increase the amount of elements in the full model and therefore increase the computational effort.

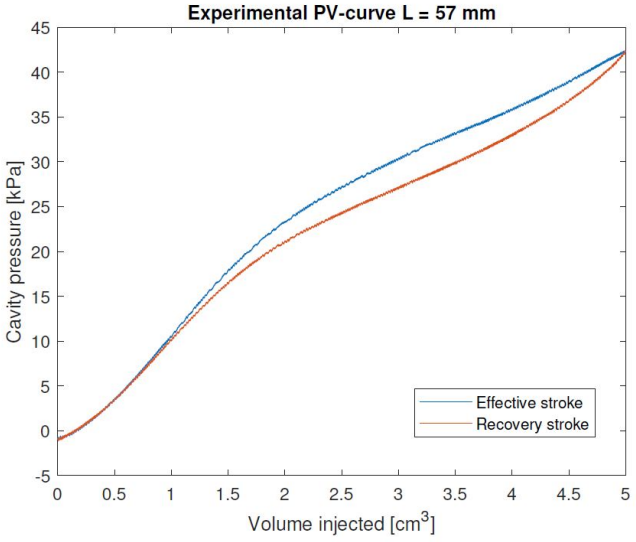

Fig. 9. The experimental pressure-volume curve for one cilium beating cycle.

The use of a coarser mesh introduces a virtual stiffness to the problem. Overall, the general shape of the experimental curve corresponds well to that of the simulated curve, this indicates that the material model does behave correctly and that the FEM-guided design is a valuable tool to realize soft bending actuator with unconventional morphologies.

VI. Conclusions and Future Work

In this paper we introduced a new design for a soft pneumatic bending actuator with an unconventional half-moon cross-section shape, which can be used as a single degree-of-freedom artificial cilium thanks to its morphological asymmetry. Through a FEM-guided design approach, we dimensionalised the half-moon actuator by assuring substantial bending deformation and structural stability. Simulations show that the corners of the half-moon are stress-free, potentially facilitating the action of the hydrodynamic forces. Moreover, the actuator has been dimensionalised to be compatible with a low Reynolds environment when submerged in glycerol for future tests as artificial cilium. In order to fabricate the actuator as a monolithic device of silicone rubber, a multi-components aluminium mold has been fabricated through a combination of wire EDM cutting and conventional milling processes. The actuator was successfully fabricated and characterized, showing a good agreement with the simulated characteristics, such as tip trajectory, bending angles and pressure-volume curve. Future works will include the use of this soft actuator as artificial cilium, to validate the hydrodynamic assumptions that lead us to formulate this peculiar design. Indeed, the rationale behind the half-moon shape is the changing hydrodynamic interaction between the effective and the recovery stroke of the cilium caused by the different surface concavity, that lead to a symmetry-breaking motion.

References

[1] B. Gorissen, E. Milana, A. Baeyens, E. Broeders, J. Christiaens, K. Collin, D. Reynaerts, and M. De Volder, "Hardware sequencing of inflatable nonlinear actuators for autonomous soft robots," *Advanced Materials*, vol. 31, no. 3, p. 1804598, 2019.

[2] M. A. Bell, L. Cattani, B. Gorissen, K. Bertoldi, J. C. Weaver, and R. J. Wood, "A soft, modular, and bi-stable dome actuator for programmable multi-modal locomotion," in *2020 IEEE/RSJ International Conference on Intelligent Robots and Systems (IROS)*. IEEE, pp. 6529–6535.

[3] C. Brennen and Howert Winet, "Fluid Mechanics of Propulsion By Cilia and Flagella," *Annu. Rev. Fluid Mech.*, vol. 9, no. Lehninger 1971, pp. 339–398, jan 1977.

[4] E. Lauga and T. R. Powers, "The hydrodynamics of swimming microorganisms," *Reports Prog. Phys.*, vol. 72, no. 9, p. 096601, sep 2009.

[5] E. M. Purcell, "Life at low Reynolds number," *Am. J. Phys.*, vol. 45, pp. 3–11, 1977.

[6] J. M. den Toonder and P. R. Onck, "Microfluidic manipulation with artificial/bioinspired cilia," *Trends in biotechnology*, vol. 31, no. 2, pp. 85–91, 2013.

[7] E. Milana, R. Zhang, M. R. Vetrano, S. Peerlinck, M. De Volder, P. R. Onck, D. Reynaerts, and B. Gorissen, "Metachronal patterns in artificial cilia for low reynolds number fluid propulsion," *Science advances*, vol. 6, no. 49, p. eabd2508, 2020.

[8] K. P. Becker, Y. Chen, and R. J. Wood, "Mechanically programmable dip molding of high aspect ratio soft actuator arrays," *Advanced Functional Materials*, vol. 30, no. 12, p. 1908919, 2020.

[9] H. Gu, Q. Boehler, H. Cui, E. Secchi, G. Savorana, C. De Marco, S. Gervasoni, Q. Peyron, T.-Y. Huang, S. Pane *et al.*, "Magnetic cilia carpets with programmable metachronal waves," *Nature communications*, vol. 11, no. 1, pp. 1–10, 2020.

[10] X. Dong, G. Z. Lum, W. Hu, R. Zhang, Z. Ren, P. R. Onck, and M. Sitti, "Bioinspired cilia arrays with programmable nonreciprocal motion and metachronal coordination," *Science advances*, vol. 6, no. 45, p. eabc9323, 2020.

[11] C. Laschi, B. Mazzolai, and M. Cianchetti, "Soft robotics: Technologies and systems pushing the boundaries of robot abilities," *Science robotics*, vol. 1, no. 1, p. eaah3690, 2016.

[12] E. Milana, B. Gorissen, S. Peerlinck, M. De Volder, and D. Reynaerts, "Artificial Soft Cilia with Asymmetric Beating Patterns for Biomimetic Low-Reynolds-Number Fluid Propulsion," *Adv. Funct. Mater.*, 2019.

[13] B. Gorissen, M. de Volder, and D. Reynaerts, "Pneumatically-actuated artificial cilia array for biomimetic fluid propulsion." *Lab Chip*, vol. 15, no. 22, pp. 4348–4355, 2015.

[14] B. Gorissen, W. Vincentie, F. Al-Bender, D. Reynaerts, and M. De Volder, "Modeling and bonding-free fabrication of flexible fluidic microactuators with a bending motion," *J. Micromech. Microeng*, vol. 23, pp. 45 012–10, 2013.

[15] J. L. Sparks, N. A. Vavalle, K. E. Kasting, B. Long, M. L. Tanaka, P. A. Sanger, K. Schnell, and T. A. Conner-Kerr, "Use of silicone materials to simulate tissue biomechanics as related to deep tissue injury," *Advances in skin & wound care*, vol. 28, no. 2, pp. 59–68, 2015.